IET Microwaves, Antennas & Propagation

Research Article

IET Journals
The Institution of Engineering and Technology

Integrated reconfigurable multiple-input–multiple-output antenna system with an ultra-wideband sensing antenna for cognitive radio platforms

ISSN 1751-8725
Received on 20th September 2014
Accepted on 30th December 2014
doi: 10.1049/iet-map.2014.0605
www.ietdl.org

Rifaqat Hussain ✉, *Mohammad S. Sharawi*

Electrical Engineering Department, King Fahd University of Petroleum and Minerals (KFUPM), Dhahran 31261, Saudi Arabia
✉ *E-mail: rifaqat@kfupm.edu.sa*

Abstract: A compact, novel multi-mode, multi-band frequency reconfigurable multiple-input–multiple-output (MIMO) antenna system, integrated with ultra-wideband (UWB) sensing antenna, is presented. The developed model can be used as a complete antenna platform for cognitive radio applications. The antenna system is developed on a single substrate area of dimensions 65×120 mm^2. The proposed sensing antenna is used to cover a wide range of frequency bands from 710 to 3600 MHz. The frequency reconfigurable dual-element MIMO antenna is integrated with P-type, intrinsic, N-type (PIN) diodes for frequency agility. Different modes of selection are used for the MIMO antenna system reconfigurability to support different wireless system standards. The proposed MIMO antenna configuration is used to cover various frequency bands from 755 to 3450 MHz. The complete system comprising the multi-band reconfigurable MIMO antennas and UWB sensing antenna for cognitive radio applications is proposed with a compact form factor.

1 Introduction

In modern wireless communications, the exponential growth of wireless services results in an increasing demand of the data rate requirements and reliability of data. These services may include high-quality audio/video calls, online video streaming, video conferencing and online gaming. These demanding features may require wide operating bandwidth (BW) or covering several frequency bands. However, frequency spectrum usage and efficiency is low and may be idle for 90% of the time [1]. This motivated work towards the efficient utilisation of the available spectrum. To overcome the inefficient and highly underutilised spectrum resources, the concept of cognitive radio (CR) has been proposed [1, 2].

A CR system is based on the structural design of a software-defined radio intended to enhance the spectrum utilisation efficiency by interacting with the operating environment. A CR-based system must be aware of its environment by sensing the spectrum usage and has the capability to switch over the operating points among different unoccupied frequency bands. The front end of a CR consists of two antennas, (i) an ultra-wideband (UWB) sensing antenna and (ii) a reconfigurable communication antenna. The UWB antenna is used to sense the entire spectrum of interest, whereas the reconfigurable antenna is used to dynamically change the basic radiating characteristics of the antenna system to utilise and operate in the available BW.

Over the past few years, reconfigurable antennas for CR applications have been investigated extensively. The focus was either on the design of reconfigurable antennas or reconfigurable communication antennas embedded with the sensing antenna. Most of the designs available in literature for wireless handheld devices are single element non-reconfigurable antennas [3–6]. In [3], a frequency-reconfigurable antenna was presented for CR platforms in wireless communication devices. The frequency band covered was from 1.64 to 2.12 GHz. The circular substrate area with radius 94 mm and height 6 mm was used for the said design implementation. In [4], a frequency reconfigurable planar inverted-F antenna (PIFA) was presented for mobile worldwide interoperability for microwave access (m-WiMAX) communication systems. The frequency ranges covered were 2.3–2.4, 2.5–2.7 and 3.4–3.6 GHz. The area of the single element PIFA was 10.5×11 mm^2 on a ground (GND) plane area of $90 \times 50 \times 6.4$ mm^3. A frequency reconfigurable antenna was proposed for mobile phone applications in [5]. The proposed PIFA design was embedded with a monopole antenna. The dimensions of the PIFA element were $4 \times 36 \times 5$ mm^3, along with a monopole antenna integrated in the same space. The proposed antenna modelled a folded-type mobile phone with two GND planes with dimensions 40×70 mm^2 and 40×70 mm^2, respectively. The frequency bands covered by the PIFA were long term evolution (LTE) (698–806 MHz) and GSM900 (880–960 MHz), whereas the monopole antenna was used for PCS1900 (1.85–1.99 GHz) and m-WiMAX (3.4–3.8 GHz) and wireless local area network (WLAN) (5.15–5.35 GHz).

Since CR front ends require sensing the frequency spectrum of the environment as well as provide narrow band reconfigurable antenna operation, the wider band sensing antenna along with the narrower band one were proposed in different ways in the literature. In [7], two different structure antennas were presented, one structure was an UWB antenna covering 3.1–11 GHz and the other was a triangular-shaped frequency reconfigurable antenna. The substrate size of the proposed antenna was 58×65.5 mm^2. In [8], a single optically controlled reconfigurable antenna was proposed for CR platforms. Four bands of operations were achieved, one UWB mode 2.65–10.3 GHz and three narrow bands at 3.55–5.18, 5.12–6.59 and 7.10–8.01 GHz. The total area of the substrate used was 33.54×49 mm^2.

In [9], a dual antenna structure was proposed for CR application with a total substrate size of 50×70 mm^2. The UWB sensing antenna was designed to operate in the frequency range from 2.1 to 10 GHz. The reconfigurability was achieved by rotational motion of a stepper motor connecting different radiating parts with input. Five different bands were obtained, 2.1–3, 3–3.4, 3.4–5.56, 5.4–6.2 and 6.3–10 GHz. The design was bulky and not suitable for mobile terminals. Several other designs were reported in the literature containing both sensing and reconfigurable antennas on the same substrate covering frequency bands above 2 GHz [10–12].

Multiple-input–multiple-output (MIMO) technology is being utilised in 4G wireless standards and beyond to achieve higher data throughput in multipath wireless channels. Thus, the use of multiple antenna elements and characterising their performance is

an inevitable task in modern antenna design [13, 14]. Several works focused on MIMO frequency reconfigurable antennas without the sensing antenna for CR applications such as those in [15–17]. Two-element MIMO antennas with two sensing antennas were presented in [18]. It was operating in the frequency band between 3 and 6 GHz with dimensions of $70 \times 80\ mm^2$. In [19], a reconfigurable MIMO filtenna was presented for CR applications along with sensing antenna for interweave and underlay CR systems. The reconfigurable antenna structure was integrated with a band-pass filter for interweave system and a band-reject filter for underlay system. The proposed designs were realised on substrate area of $70 \times 80\ mm^2$ for interweave system and $65 \times 70\ mm^2$ for underlay system. Both the sensing and the reconfigurable antennas were designed for frequency range 3–6 GHz.

Most of the works related to CR applications with reconfigurable antenna systems cited in the literature were single element with a sensing antenna working above 2 GHz and very few designs with MIMO antenna operation were proposed that were above 3 GHz.

In this work, a novel modified reconfigurable PIFA-like MIMO antenna is proposed for CR applications. This two-element MIMO system is embedded with P-type, intrinsic, N-type (PIN) diodes to tune the antenna over various frequency bands. The distinguishing feature of the proposed design is its operation at low-frequency bands starting from 755 MHz and going up to 3450 MHz, based on the selection of reconfiguration mode. Moreover, another interesting feature of the proposed design is the integration of an UWB sensing antenna with low operating frequency with the reconfigurable MIMO antenna system without any significant addition to the planar structure. The GND plane of the MIMO PIFA is optimised and tuned to work as a sensing antenna during the scanning phase of the frequency spectrum and operates as a GND reference plane during the communication stage. All of the designs known so far use separate sensing and reconfigurable MIMO antennas in CR applications. Furthermore, the proposed MIMO antenna system is compact and suitable for handheld (smart phones, tablets and personal digital assistants) CR platforms with MIMO capability.

2 Design details

The proposed novel frequency reconfigurable modified PIFA MIMO antenna system along with its UWB sensing antenna is shown in Figs. 1*a* and *b*. The complete model consists of two printed circuit boards. The main board with dimensions $65 \times 120 \times 1.56\ mm^3$ containing the UWB sensing antenna on the bottom layer and GND plane of the UWB monopole antenna on the top side of the main board. The elevated board containing the modified PIFA MIMO reconfigurable antennas each with dimensions $30 \times 12 \times 0.8\ mm^3$. Both designs were fabricated on a commercial FR-4 substrate with $\varepsilon_r = 4.4$. Fig. 1*c* shows the side view, whereas Fig. 1*d* shows the front view of the reconfigurable antenna. Both elements were connected to the GND plane through a shorting wall of width 1.7 mm. Fig. 1*c* is zoomed in to show the shorting wall from the bottom of the elevated antenna to the GND plane. The shorting walls connecting the elevated antenna with the GND plane was used to lower the resonating frequencies of the elements.

The reconfigurable MIMO elements were mounted on the top corners of the main board with a coaxial feed (the conducting pin of the SMA connector is soldered to the bottom layer of the MIMO antenna elements at its feeding point, which also holds the board precisely at correct height. Styrofoam is used to maintain the height of the elevated board). The total height of the whole system was 5.8 mm. The bottom layer of the main board contained the UWB monopole antenna which was also acting as a reference GND plane for the reconfigurable antennas. Fig. 2*a* shows the top view of the two reconfigurable modified PIFA MIMO elements with their associated digital biasing circuitry. PIN diodes were used to connect the two different radiating parts at two different points on the top side of elements, thus providing reconfigurability. The switching mechanism of the PIN diodes leads to four distinct modes of operation for each element. Fig. 2*b* shows the bottom layer of the reconfigurable MIMO antenna elements. The bottom side consists of radiating lines and the coaxial feed. The two elements were fed from the bottom side. Figs. 2*c* and *d* show the top and bottom views of the fabricated

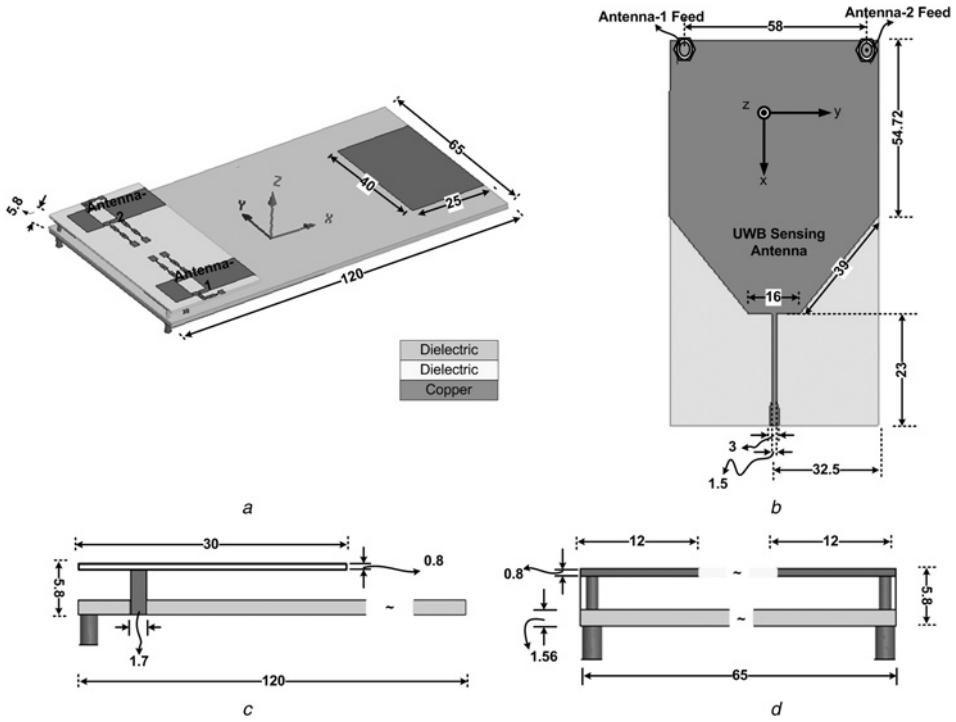

Fig. 1 *Proposed MIMO antennas system for CR platform*

a Top view
b Bottom view
c Side view
d Front view
All dimensions are in millimetre (mm)

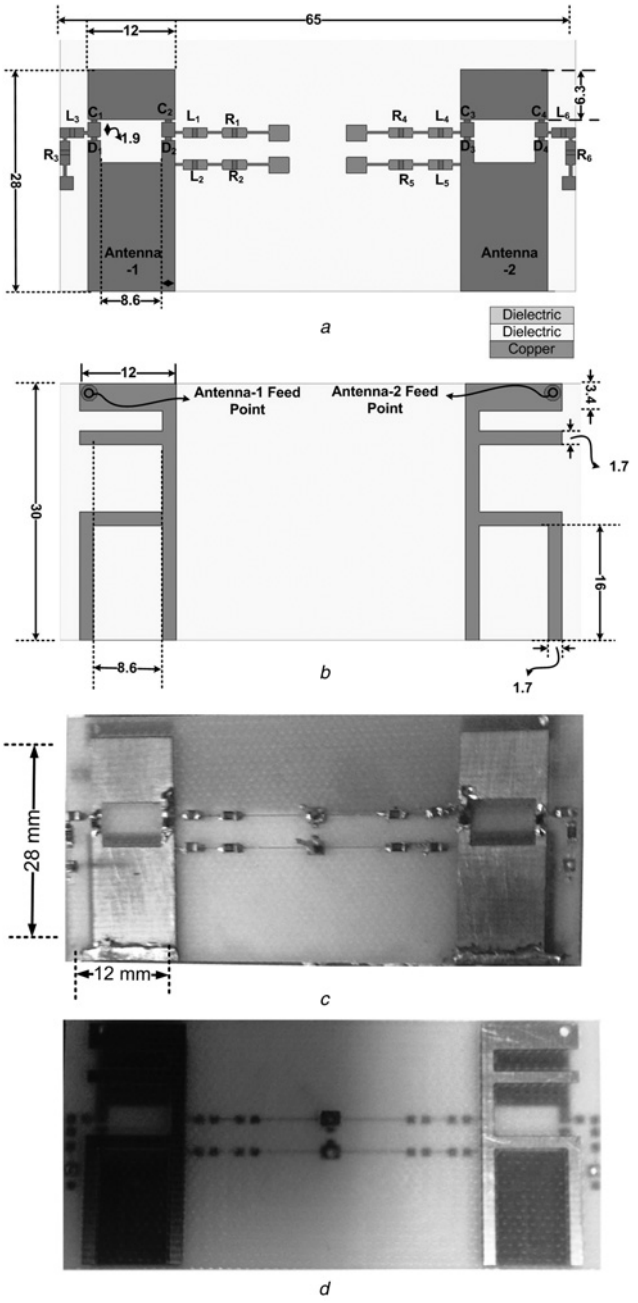

Fig. 2 *Detailed schematic of the two-element reconfigurable MIMO antenna*

a Top view
b Bottom view
c Top view of fabricated antenna
d Bottom view of fabricated antenna
All dimensions are in millimetre (mm)

modified PIFA reconfigurable MIMO antennas, respectively. The design procedure of the proposed structure was started with an inverted F-shaped antenna of certain length elevated at certain height without any substrate. The given structure was tuned to resonate above 2 GHz with dimensions 12×30 mm^2. This design was compact but was operating at higher frequency bands with single resonance. The F-shape architecture was added with a meandered line to provide additional paths for the current and hence to achieve more than one resonating mode. For mobile application and other wireless handheld devices, the antenna size should be compact with low-frequency bands of operation as well. Hence, the antenna structure was further modified, by folding the structure on the top of the substrate with a planar structure. The total length of the antenna was optimised to cover lower frequency bands as well but without reconfigurability. A rectangular slot was created on the top layer to enhance the BW as well as to provide different current paths to achieve reconfigurability by a switching mechanism. Furthermore, two small slots were created in the arms of the rectangular slot to add the PIN diodes for switching. Extensive parametric analyses were performed to optimally place the rectangular slot as well as the position of PIN diodes for maximum bands coverage.

The biasing circuitry for a single diode is shown in Fig. 3*a*. Two diodes were used for each antenna. The circuit is a series combination of an radio-frequency (RF) choke of 1 μH in series with 2.1 kΩ resistor connecting the PIN diode with the radiating part of antenna. Both terminals of the PIN diode were connected with the resistor–inductor circuit to isolate the DC and RF parts of the antenna. The value of the resistor is selected to pass sufficient and within the rating current in the forward biased condition through PIN diode. The two reconfigurable antennas are exactly similar in structure to form the MIMO system. All the resistor, capacitor and inductor values used in the biasing circuitry were same for all four branches containing the PIN diodes for switching purposes.

The fabricated model of the proposed design is shown in Figs. 3*b* and *c*. Fig. 3*b* shows the top view of the complete two-element

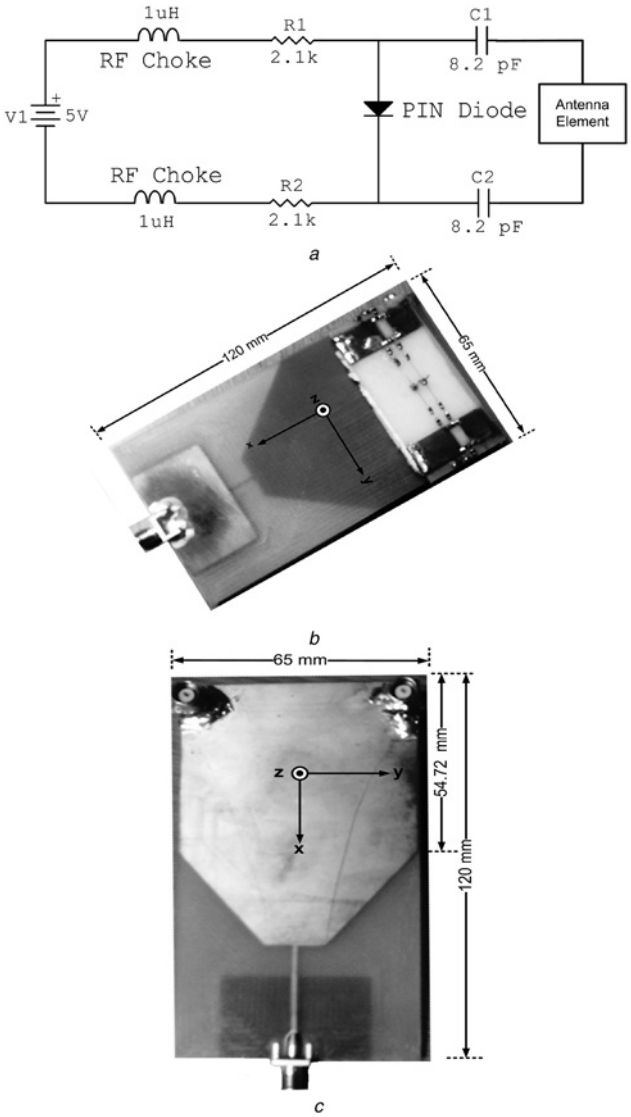

Fig. 3 *Biasing circuitry and fabricated antenna model*

a PIN diode biasing circuitry
b Top view of fabricated model
c Bottom view of fabricated model

MIMO antenna system integrated with the UWB sensing antenna. Fig. 3*c* shows the bottom layer of the fabricated sensing antenna which was also acting as a reference GND plane for the reconfigurable antenna.

3 Simulation and measurement results

The complete two element reconfigurable MIMO antenna system along with its sensing antenna was modelled and optimised using the HFSS™. The optimised design was fabricated using an LPKF-Protomat S103. The scattering parameters of the fabricated design were measured using an Agilent N9918A vector network analyser. The gain patterns and efficiencies were measured at King Abdullah University of Science and Technology (KAUST), Jeddah, Saudi Arabia, using a SATIMO Starlab anechoic chamber. The starting frequency for the chamber was 800 MHz. All measured and simulated results of MIMO antennas and sensing antennas are summarised in the following subsections.

3.1 UWB sensing antenna

An UWB sensing antenna is an essential and integral part of CR platforms for channel sensing. The proposed UWB sensing antenna is based on a monopole structure as shown in Fig. 1*b*. The objective of this work was to achieve UWB sensing operation bands of 700–3500 MHz with typical smart mobile handset backplane size of $65 \times 120\ mm^2$. The design presented cover frequency bands from 710 to 3600 MHz. According to the literature survey conducted, most of the UWB designs for CR platform were operating above 3 GHz and very few were found to be working in the 2 GHz and above keeping in mind the area constraint.

The simulated and measured reflection coefficients are shown in Fig. 4*a*. The measured results for the fabricated antenna are in close agreement with the simulated results. To check the effect of having a hand on the UWB antenna, a curve showing the resonance behaviour in its presence has little effect on the antenna s_{11} curves.

The reconfigurable communication antenna is integrated with sensing antenna by sharing the same substrate and is critical to consider the mutual coupling or isolation between the

Table 1 Antenna efficiency and PG of the sensing antenna

	PG, dBi		Efficiency, %	
	Simulated	Measured	Simulated	Measured
800 MHz	2.72	3.19	75	67
1500 MHz	4.01	5.49	91	84
3000 MHz	4.69	3.79	96	87

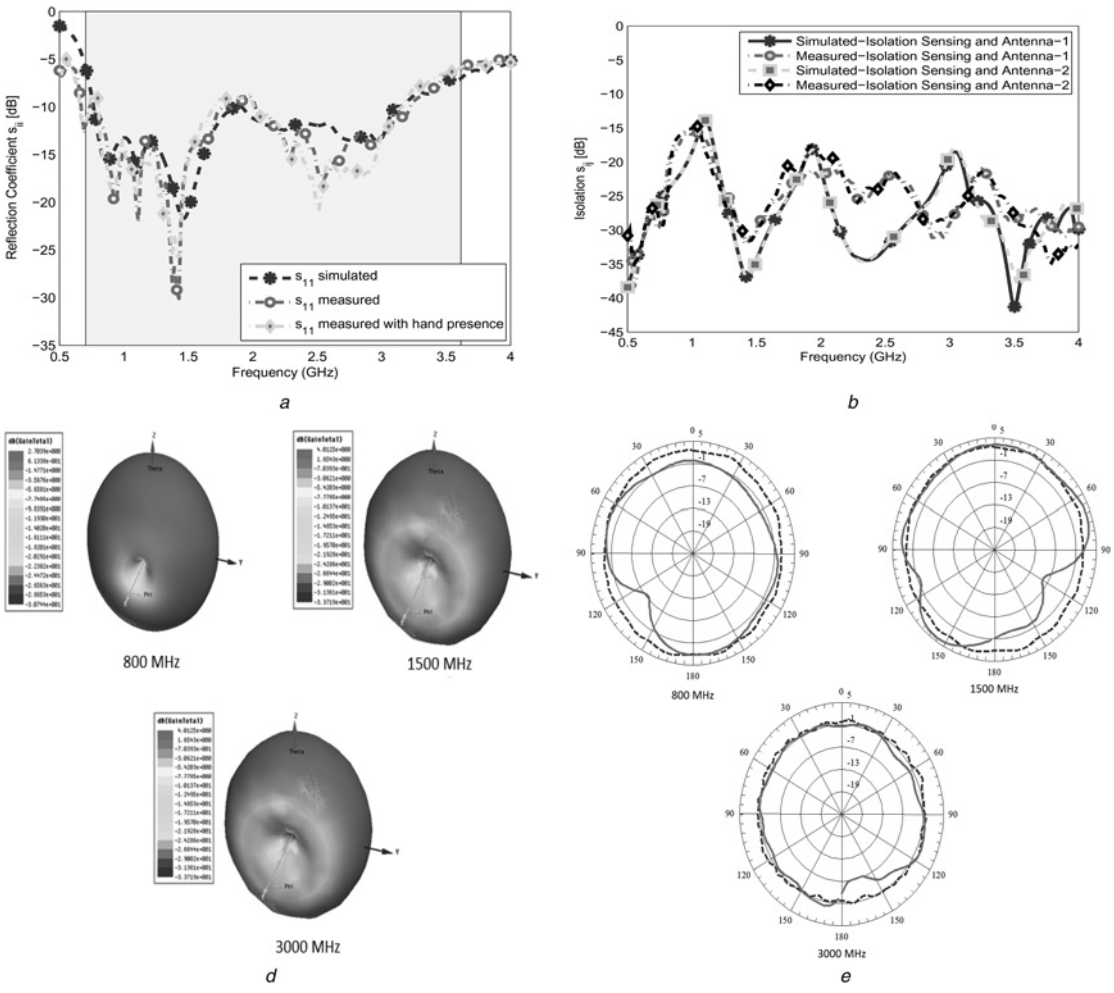

Fig. 4 *Reflection coefficients, mutual coupling and gain patterns*

a Simulated and measured reflection coefficient of UWB sensing antenna
b Mutual coupling between sensing and MIMO antennas
c Simulated 3D gain patterns
d Simulated and measured 2D gain pattern in *yz*-plane
Dashed lines – simulated, solid lines – measured

Table 2 Reconfigurable antenna operation modes

S. no.	PIN diode 2	PIN diode 1
mode-1 (M1)	OFF	OFF
mode-2 (M2)	OFF	ON
mode-3 (M3)	ON	OFF
mode-4 (M4)	ON	ON

communication and sensing antennas. Fig. 4*b* shows the isolation between (the measured and simulated $|s_{21}|$ curves between the MIMO and UWB antenna ports) sensing antenna and the two-element MIMO antennas. It has been observed that the minimum isolation is better than 14 dB in all frequency bands (note that the antennas are assumed to operate in a sequential mode, i.e. sensing, and then using that band, thus lower coupling is expected). The sensing antenna for CR applications must possess an omnidirectional radiation pattern. Fig. 4*c* shows the simulated three-dimensional (3D) gain patterns of the UWB antenna at three different frequency bands: 800, 1500 and 3000 MHz, respectively. The simulated and measured 2D gain patterns in the *yz*-plane at three different frequencies (800, 1500 and 3000 MHz) are shown in Fig. 4*d*. The peak gain (PG) and efficiencies for sensing antenna are computed. The simulated and measured results are given in Table 1. Good agreement is observed.

3.2 Reconfigurable MIMO antenna

Each reconfigurable MIMO element is based on modified PIFA consisting of folded patch with a meander line structure. The bottom side meander structure provides two different current paths resulting in multi-resonances. The top side of the modified PIFA is a discontinuous slotted patch antenna structure. The discontinuity of the antenna is integrated with PIN diodes for connecting or disconnecting the two top parts of the antenna structure. Thus, diodes are used to provide more flexibility by its ON/OFF operation. The non-symmetrical structure of the PIFA with PIN diodes results in different radiating lengths which results in multiple bands for various modes of operation. The two PIN diodes in each antenna element result in four distinct operating modes for each MIMO antenna element. The details of modes for PIN positions are given in Table 2. These four modes of operation result in different frequency resonances. These modes are:

(i) *Mode-1:* In this mode, both PIN diodes at the top side of the reconfigurable MIMO antenna are switched OFF. The resulted simulated and measured reflection coefficients of mode-1 are shown in Fig. 5*a*. In mode-1, the MIMO reconfigurable antenna is resonating at three different bands. The first resonance occurs at 1095 MHz, whereas the second and third resonances occur at 1945 and 3050 MHz with a −6 dB operating BW of at least 44 MHz in all three bands. A slight shift is observed in the measurement of the third resonance because of the fabrication tolerances that became more significant at higher frequencies.
(ii) *Mode-2*: In this mode, PIN diode 1 is switched ON, whereas PIN diode 2 is switched OFF. The resulted simulated and measured reflection coefficients are shown in Fig. 5*b*. In mode-2, the antenna resonates at two different bands. The first resonance occurs at 770 MHz whereas the second resonance occurs at 1660 MHz with a −6 dB operating BW of at least 30 MHz in both bands.
(iii) *Mode-3*: In this mode, PIN diode 1 is switched OFF, whereas PIN diode 2 is switched ON. The resulted simulated and measured reflection coefficients are shown in Fig. 5*c*. In mode-3, the antenna is resonating at four different bands. The first resonance occurs at 1000 MHz, whereas the second, third and fourth resonances occur

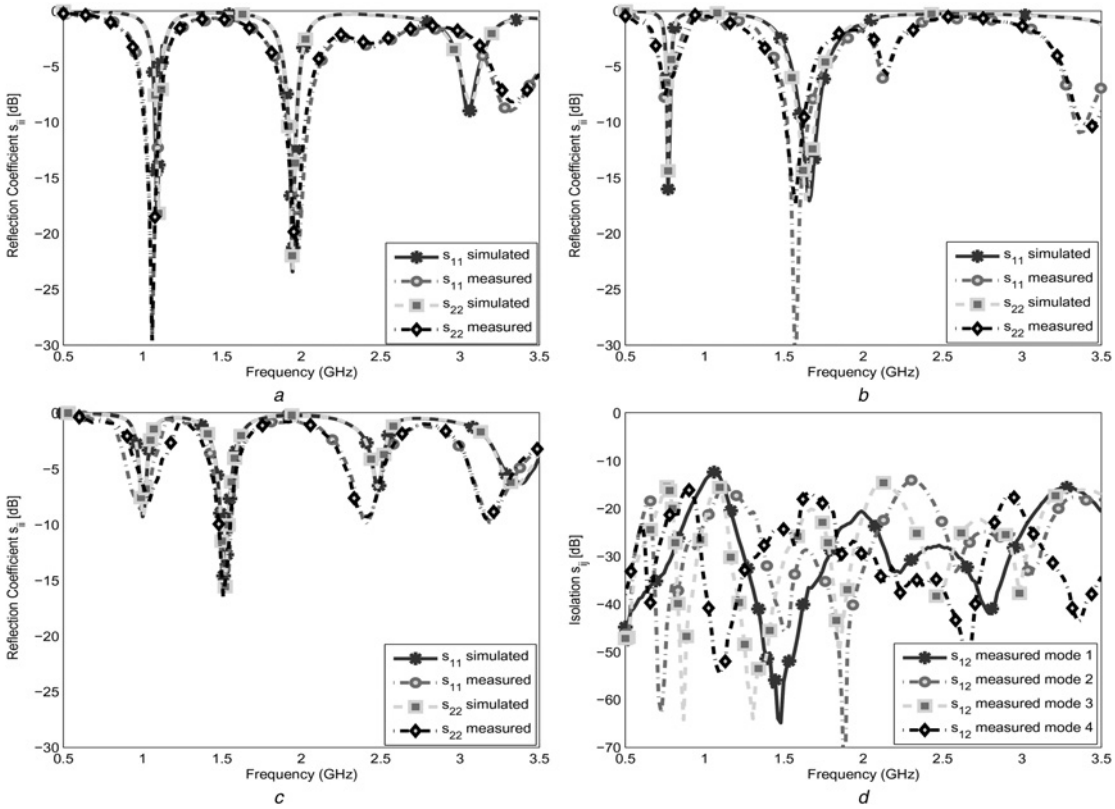

Fig. 5 *Reflection coefficients and isolation curves*

a Reflection coefficients of the MIMO antenna system – mode-1
b Reflection coefficients of the MIMO antenna system – mode-2
c Reflection coefficients of the MIMO antenna system – mode-3
d Measured isolation between MIMO antenna elements

IET Microw. Antennas Propag., 2015, Vol. 9, Iss. 9, pp. 940–947

Table 3 Measured reconfigurable antenna bands, centre frequency (f_c in MHz) and BW (in MHz) for antenna-1 (A1), antenna-2 (A2), all modes (M1, M2, M3, M4)

		Band-1		Band-2		Band-3		Band-4	
		f_c	BW	f_c	BW	f_c	BW	f_c	BW
M1	A1	1060	80	2018	130	3195	160	—	—
	A2	1065	80	2020	130	3195	160	—	—
M2	A1	747	60	1583	210	—	—	—	—
	A2	751	65	1580	220	—	—	—	—
M3	A1	995	110	1510	130	2410	155	3250	160
	A2	1020	110	1515	130	2420	150	3250	160
M4	A1	975	75	1690	210	—	—	—	—
	A2	980	75	1675	215	—	—	—	—

at 1508, 2450 and 3350 MHz with a −6 dB operating BW of at least 44 MHz in all four bands.

(iv) *Mode-4:* In this final mode, both PIN diodes at the top side of MIMO antenna are switched ON. In mode-4, the MIMO antenna resonates at 1060 and 1760 with a −6 dB operating BW of 50 and 180 MHz, respectively.

The details of the measured centre resonance frequencies (f_c in MHz) and −6 dB operating BW (in MHz) of the reconfigurable MIMO antenna system are shown in Table 3 for all modes.

From the measured and simulated results, it is evident that close agreement is found between them. The differences in the simulated and measured results were mainly because of the differences in substrate properties of the fabricated antenna and fabrication tolerances. In higher frequency bands, the shift in the frequency was because of the PIN diodes used in the circuit. The fabricated model used PIN diodes, BAP50-02, that can work up to 3 GHz, but we used them up to 3.6 GHz. The insertion loss $|s_{12}|$ of the diode rises significantly above 3 GHz and hence had an adverse effect on its performance above this maximum frequency. In addition, the shift may be because of the lack of modelling flexibility of PIN diodes in HFSS. The diodes were modelled as resistive circuits in forward bias while becoming a capacitive circuits in reverse bias conditions according to their data sheets. The circuit model of a PIN diode in forward and reverse bias conditions can be resembled by a simple resistor and capacitor, respectively. Having a fixed value for this, the bias condition is not totally accurate as it is also a function of frequency. The frequency dependence of the resistive and capacitive values of a PIN diode cannot be easily modelled in HFSS, since it is not a circuit simulator. This causes some slight shift in the frequency response at various frequency points. But the use of a single value for the forward and reverse bias conditions resulted in very good agreement between simulated/modelled and measured results for this design.

For the MIMO antenna system, mutual coupling between MIMO antenna elements is important to consider. The measured isolation between MIMO elements is shown in Fig. 5*d* for all four modes. The worst-case isolation was 12 dB between the MIMO antenna elements for both simulated and measured values. The obtained isolation values are acceptable for good MIMO operation. It should be noted that for such multi-band highly compact antennas, it is difficult to guarantee excellent isolation at all bands.

3.3 Current distribution

The proposed reconfigurable MIMO antenna system was also analysed from its surface current densities obtained from HFSS simulations as shown in Fig. 6. The analysis presented here is only for mode-1 and can be extended to other modes of operation as well. The current density analysis presented here for mode-1 at three frequency bands. Fig. 6*a* shows the current density on the top and bottom surfaces of antenna-2 as well as on the reference GND plane of MIMO antenna at its first resonance of 1095 MHz while antenna-1 and the sensing antennas were terminated with 50 Ω. As evident from the figures, a high current density was along the inner side of the meander line and the inner edge of the folded patch at the top side. The GND plane also acts as a part of the radiator as the bottom side of PIFA is connected directly to the GND plane. There is slight coupling on the bottom and top sides of the antenna-1 while the coupling through the GND plane is insignificant. Similar behaviour was observed with the excitation of antenna-1 at 1095 MHz. Similarly, Figs. 6*b* and *c* show the current distributions at 1945 and 3050 MHz, respectively.

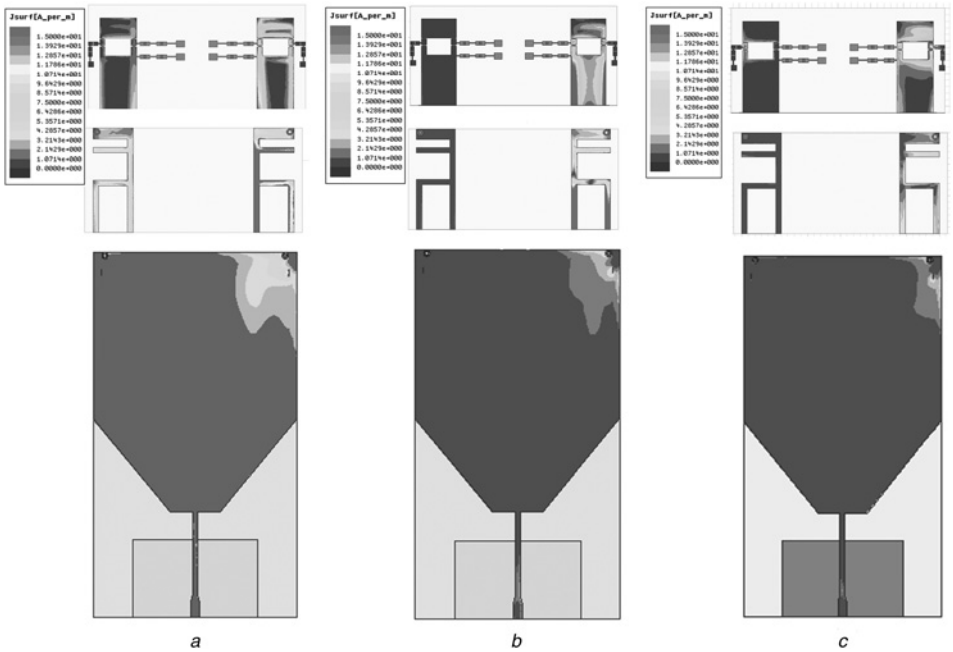

Fig. 6 *Current distribution for the MIMO antenna system*

a 1095 MHz – antenna-2 excited
b 1945 MHz – antenna-2 excited
c 3050 MHz – antenna-2 excited

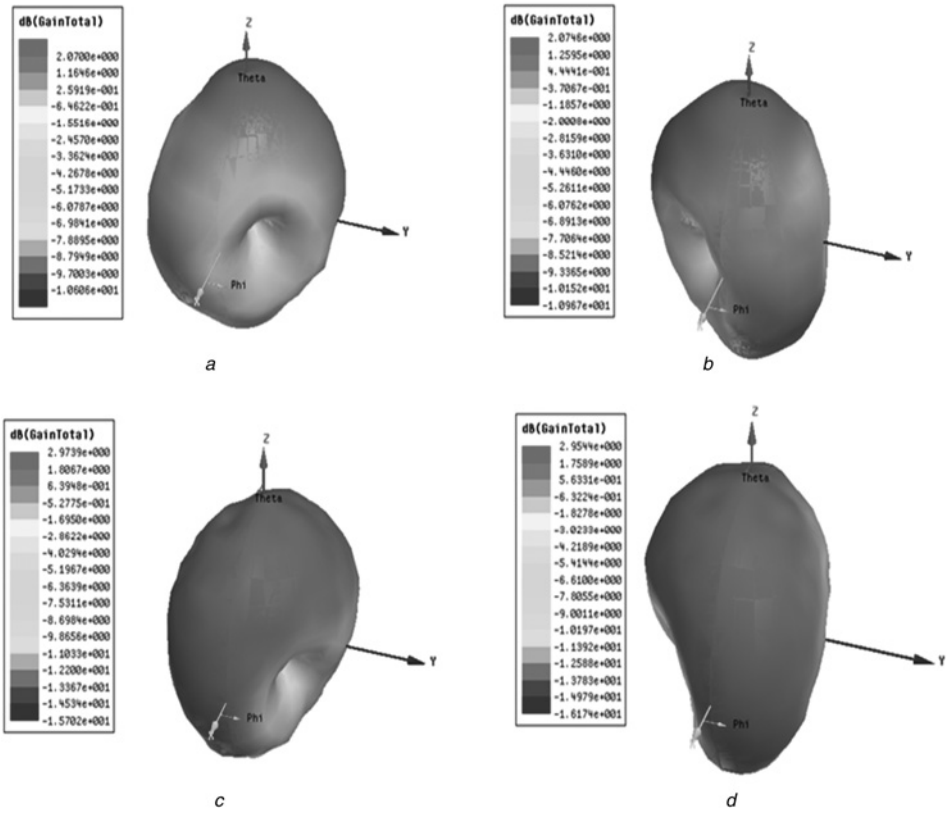

Fig. 7 *Simulated 3D gain pattern mode-1*

a Antenna-1 excited at 1095 MHz
b Antenna-2 excited at 1095 MHz
c Antenna-1 excited at 1945 MHz
d Antenna-2 excited at 1945 MHz

3.4 Far field radiation characteristics of the reconfigurable MIMO antenna

The 3D radiation patterns of the proposed reconfigurable MIMO antenna system were computed using the HFSS. The gain patterns for each mode and each band were obtained for one element while the second was terminated with 50 Ω. The gain patterns of the first mode are shown in Fig. 7 at its two-operating bands. In Fig. 7, the 3D gain pattern is plotted for two bands: 1095 and 1945 MHz. Figs. 7*a* and *b* show the gain patterns of antenna-1 and antenna-2, respectively at 1095 MHz. Similarly, Figs. 7*c* and *d* show the gain patterns of two antennas at 1945 MHz. The maximum of each element is tilted showing lower field correlation that is usually desired.

The 2D measured gain patterns of the MIMO antenna systems are presented here for two modes at single frequency. Figs. 8*a* and *b* show the normalised measured gain patterns of the proposed MIMO antenna system at 3195 MHz of mode-1. The maximum measured gain at this frequency was 3.2 dBi. All co-pol and cross-pol patterns for the two elements of the MIMO antenna are given in Figs. 8*a* and *b*, respectively. Figs. 8*c* and *d* show the measured gain pattern at 1580 MHz of mode-2. All co-pol and cross-pol patterns are given in Figs. 8*c* and *d*, respectively.

The simulated and measured PGs in dBi and %η are given in Table 4 for all modes of operation. It should be noted that the low efficiency at some bands is because of the fact that this multi-resonate antenna depends on higher order modes for these bands in addition to the fact that the design is fabricated on a

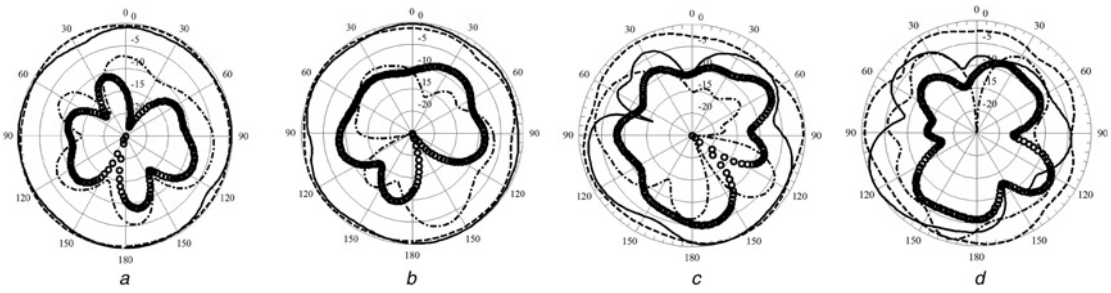

Fig. 8 *Measured normalised gain patterns for the proposed MIMO antenna mode-1 and mode-2*

a *xz*-plane at 3195 MHz
b *yz*-plane at 3195 MHz
c *xz*-plane at 1580 MHz
d *yz*-plane at 1580 MHz
Solid: co-pol element 1; dashes: co-pol element 2; circle: cross-pol element 1; and dashes-dot: cross-pol element 2

IET Microw. Antennas Propag., 2015, Vol. 9, Iss. 9, pp. 940–947

Table 4 Simulated and measured PGs (in dBi) and radiation efficiencies (η%)

		Band-1				Band-2				Band-3				Band-4			
		Simulated		Measured		Simulated		Measured		Simulated		Measured		Simulated		Measured	
		PG	η%	PG	η%	PG	η%	PG	η%	PG	η%	PG	η%	PG	η%	PG	η%
M1	A1	0.54	40	−1.2	26	2.99	55	1.56	41	5.2	62	3.2	45	–	–	–	–
	A2	0.55	40	−1.5	27	3.15	56	1.42	41	5.2	62	3.05	47	–	–	–	–
M2	A1	−5.01	22	–	–	3.1	75	2.03	60	–	–	–	–	–	–	–	–
	A2	−5.03	22	–	–	3.12	74	2.03	61	–	–	–	–	–	–	–	–
M3	A1	−3.13	26	−5.23	20	2.25	58	0.27	34	2.53	25	1.25	20	1.53	40	0.12	25
	A2	−3.13	26	−5.23	20	2.25	58	0.26	35	2.53	25	1.23	19	1.53	41	0.132	254
M4	A1	−1.56	37	−2.56	23	3.53	60	2.01	46	–	–			–	–	–	–
	A2	−1.62	35	−2.7	24	3.54	61	1.97	46	–	–	–	–	–	–	–	–

Table 5 Simulated and measured envelope correlation coefficient (ρ_e) for all bands (B-1, B-2, B-3, B-4)

	Simulated results				Measured results			
	B-1	B-2	B-3	B-4	B-1	B-2	B-3	B-4
M1	0.0.0289	0.01	0.004	–	0.0049	0.625	0.009	–
M2	0.0144	0.00366	–	–	–	0.0144	–	–
M3	0.0289	0.0016	0.001	0.0025	0.009	0.17	0.09	0.02
M4	0.009	0.001	–	–	0.015625	0.00625	–	

lossy substrate (FR-4). The low-efficiency values leads to negative gain values in dB. This can be compensated for using active circuits in the transmit and receive paths of the system.

Envelope correlation coefficient values for both measured and simulated data are summarised in Table 5. It is clear that the proposed reconfigurable MIMO antenna system with an integrated UWB antenna for CR applications will satisfy the ρ_e values required for good MIMO operation. Some measured values of ρ_e are missing because of the lower end frequency limitation in the Satimo chamber.

4 Conclusion

A novel compact reconfigurable MIMO antenna system integrated with an UWB sensing antenna is presented. The proposed antenna design is suitable for CR applications in small wireless handheld devices. It covers various frequency bands at the lower end of the RF spectrum. The sensing antenna covered frequency bands from 710 to 3600 MHz. The reconfigurable multi-band, multi-mode antenna covered several frequency bands between 755 and 3450 MHz. The operating BW in all modes was at least 30 MHz. The antenna was also evaluated for MIMO parameters where it showed good performance. The total space occupied by whole design was $65 \times 120 \times 5.8$ mm^3, which is very compact given the covered frequencies.

5 Acknowledgments

The authors acknowledge the support provided by the King Abdul Aziz City for Science and Technology (KACST) and the Science and Technology unit at King Fahd University of Petroleum and Minerals (KFUPM) for funding this work through the project No. 12-ELE3001-04, as part of the National Science, Technology and Innovation Plan (NSTIP). Also, they acknowledge the help of Prof. A. Shamim of KAUST for granting access to the measurement facility.

6 References

1 Mitola, J.: 'Cognitive radio architecture evolution', *Proc. IEEE*, 2009, **97**, (4), pp. 626–641
2 Haykin, S.: 'Cognitive radio: brain-empowered wireless communications', *IEEE J. Sel. Areas Commun.*, 2005, **23**, (2), pp. 201–220
3 Ge, L., Luk, K.M.: 'Frequency-reconfigurable low-profile circular monopolar patch antenna', *IEEE Trans. Antennas Propag.*, 2014, **62**, (7), pp. 3443–3449
4 Lim, J.H., Song, C.W., Jin, Z.J., Yun, T.-Y.: 'Frequency reconfigurable planar inverted-F antenna using switchable radiator and capacitive load', *IET, Microw. Antennas Propag.*, 2013, **7**, (6), pp. 430–435
5 Cho, J., Jung, C., Kim, K.: 'Frequency-reconfigurable two-port antenna for mobile phone operating over multiple service bands', *Electron. Lett.*, 2009, **45**, (20), pp. 1009–1011
6 Chattha, H.T., Nasir, M., Abbasi, Q.H., Huang, Y., Aljaafreh, S.S.: 'Compact low profile dual port single wideband planar inverted-F MIMO antenna', *Antenna Wirel. Propag. Lett.*, 2013, **12**, pp. 1673–1675
7 Tawk, Y., Christodoulou, C.: 'A new reconfigurable antenna design for cognitive radio', *IEEE Antennas Wirel. Propag. Lett.*, 2009, **8**, pp. 1378–1381
8 Jin, G., Zhang, D., Li, R.: 'Optically controlled reconfigurable antenna for cognitive radio applications', *Electron. Lett.*, 2011, **47**, (17), pp. 948–950
9 Tawk, Y., Costantine, J., Avery, K., Christodoulou, C.: 'Implementation of a cognitive radio front-end using rotatable controlled reconfigurable antennas', *IEEE Trans. Antennas Propag.*, 2011, **59**, (5), pp. 1773–1778
10 Ebrahimi, E., Hall, P.S.: 'A dual port wide-narrowband antenna for cognitive radio'. IEEE Third European Conf. on Antennas and Propagation, 2009, pp. 809–812
11 Ghanem, F., Hall, P., Kelly, J.: 'Two port frequency reconfigurable antenna for cognitive radios', *Electron. Lett.*, 2009, **45**, (11), pp. 534–536
12 Hamid, M.R., Gardner, P., Hall, P.S., Ghanem, F.: 'Reconfigurable vivaldi antenna', *Microw. Opt. Technol. Lett.*, 2010, **52**, (4), pp. 785–787
13 Sharawi, M.S.: 'Printed multi-band MIMO antenna systems and their performance metrics', *IEEE Antennas Propag. Mag.*, 2013, **55**, pp. 218–232
14 Sharawi, M.S.: 'Printed MIMO antenna engineering' (Artech House, 2014, 1st edn.), pp. 23–36
15 Hu, Z., Hall, P., Gardner, P.: 'Reconfigurable dipole-chassis antennas for small terminal MIMO applications', *Electron. Lett.*, 2011, **47**, (17), pp. 953–955
16 Chiu, C.Y., Murch, R.D.: 'Reconfigurable multi-port antennas for handheld devices'. IEEE Int. Symp. on Antennas and Propagation Society APSURSI, 2009, pp. 1–4
17 Lim, J.H., Jin, Z.J., Song, C.W., Yun, T.Y.: 'Simultaneous frequency and isolation reconfigurable MIMO PIFA using pin diodes', *IEEE Trans. Antennas Propag.*, 2012, **60**, (12), pp. 5939–5946
18 Tawk, Y., Costantine, J., Christodoulou, C.: 'A MIMO cognitive radio antenna system'. IEEE Antennas and Propagation Society (APSURSI), 2013
19 Tawk, Y., Costantine, J., Christodoulou, C.: 'Reconfigurable filtennas and MIMO in cognitive radio applications', *IEEE Trans. Antennas Propag.*, 2014, **62**, (3), pp. 1074–1084